The Sonochemical Degradation of Azobenzene and Related Azo Dyes: Rate Enhancements via Fenton's Reactions

Jiju M. Joseph, Hugo Destaillats, Hui-Ming Hung, and Michael R. Hoffmann*

W. M. Keck Laboratories, California Institute of Technology, Pasadena, California 91125

The sonochemical degradation of aqueous solutions of azobenzene and related azo dyes (methyl orange, *o*-methyl red, and *p*-methyl red) was performed at 500 kHz and 50 W, under air, O_2, or Ar saturation at 288 K. Reaction products and intermediates were identified by HPLC-ES-MS. Total organic carbon (TOC) was also determined as a function of reaction time. We propose a reaction mechanism based on the observed species and the extent and rate of TOC depletion. The addition of OH radicals to the azo double bond is considered to be the first step of the sequence of oxidative bond cleavages leading to the production of carboxylic acids, quinones, carbon dioxide, and nitrate ions as the main degradation products. The effects of the dye structures and of the background gas on the sonochemical bleaching rates were also investigated. The reaction rates for *o*-methyl red were approximately 30–40% faster than those for the other compounds. This appears to be a strong influence by a carboxylic group ortho to the azo group. Saturating with Ar instead of air or O_2 increased the pseudo first-order rate constants for the degradation by 10%. The acceleration of the sonochemical bleaching and the mineralization process upon addition of Fe(II) was also investigated in Ar-saturated methyl orange solutions. A 3-fold increase in the reaction rate was observed at optimal Fe(II) concentrations. This kinetic effect is quantitatively accounted for by a simple kinetic model based on the reaction of Fe(II) with sonochemically produced H_2O_2 (Fenton's reaction). This latter effect illustrates a simple way of achieving a substantial improvement in the efficiency of sonochemical degradation reactions.
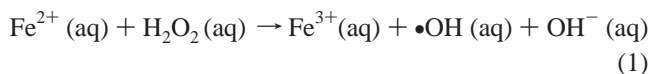
Introduction

Sonochemistry has emerged in the past years as an advanced oxidation process for the destruction of hazardous organic compounds in aqueous solutions.[1–5] Ultrasonic irradiation induces the production of cavitation bubbles in the liquid through which it is transmitted. These microbubbles grow during the subsequent compression–rarefaction cycles until they reach a critical size. Further compression leads to the collapse of the bubbles, with the concomitant release of heat and production of chemically active species during the last phase of the bubble collapse. The chemical effects are a direct result of the very high temperatures, on the order of 4000–5000 K, and pressures, in the range of hundreds of bars, that are reached in the gaseous cavities when the size of the cavities is reduced many orders of magnitude within a few microseconds.[6–8] Under such extreme conditions, the water molecules present inside the bubble dissociate yielding •OH (g) and •H (g) radicals. The radical species produced can either recombine, react with other gaseous species present in the cavity, or diffuse out of the bubble into the bulk fluid medium where they are able to react with solute molecules. A steady-state concentration of reactive radical species in the liquid phase is then generated by continuous irradiation with ultrasound.

The substrate molecules can undergo degradation by two different main pathways depending on their chemical nature: pyrolytic reactions inside the cavitation bubbles or oxidation by hydroxyl radical in the bulk medium. Supercritical phase reactions are also possible.[2] Nonvolatile compounds degrade mainly by reaction with hydroxyl radicals in the bulk solution, while those with higher vapor pressure can partition into the bubble and also undergo thermal degradation in the gas phase. The rate of sonochemical reactions is influenced by the nature of the background gas, since the temperature attained within the cavitation bubble upon collapse depends on physicochemical properties such as the polytropic ratio (C_p/C_v), thermal conductivity, and the solubility of a gas in water.[6] The yield of the free radicals formed depends essentially on the temperature reached within the bubble in the final collapse stages.[7–9]

Many efforts have been devoted to improve the efficiency of sonochemical reactions, considering that a substantial amount of the energy employed in generating the radicals is not effectively converted into an optimum yield of the desired products.[10–12] The recombination of •OH to yield H_2O_2 both in the gas phase within the bubbles and in solution are two of the major processes that limit the amount of reactive radicals accessible to the target molecules. The sonochemically generated H_2O_2 in most cases is not able to react with them and eventually decomposes. Therefore, the addition of $FeSO_4$ to the treated solutions is studied in the present work as a way to enhance the amount of •OH available in solution. The classical Fenton's reaction[13,14]

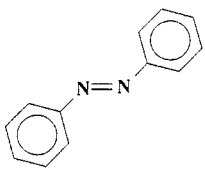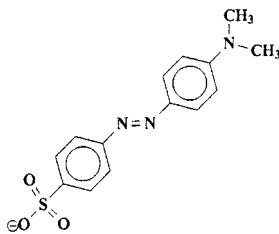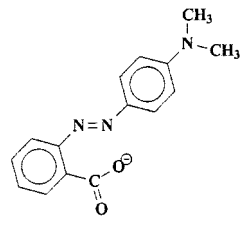$$Fe^{2+}(aq) + H_2O_2(aq) \rightarrow Fe^{3+}(aq) + \bullet OH(aq) + OH^-(aq) \tag{1}$$
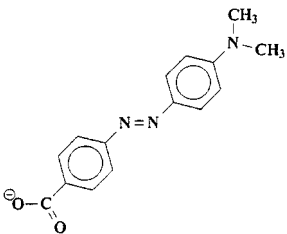
becomes a secondary source of •OH (aq), recovering part of its chemical activity otherwise lost in the production of relatively large amounts of H_2O_2 during sonication.[15] The sonochemical yield of H_2O_2 depends on the irradiation parameters (frequency and power density), temperature, and nature of the background
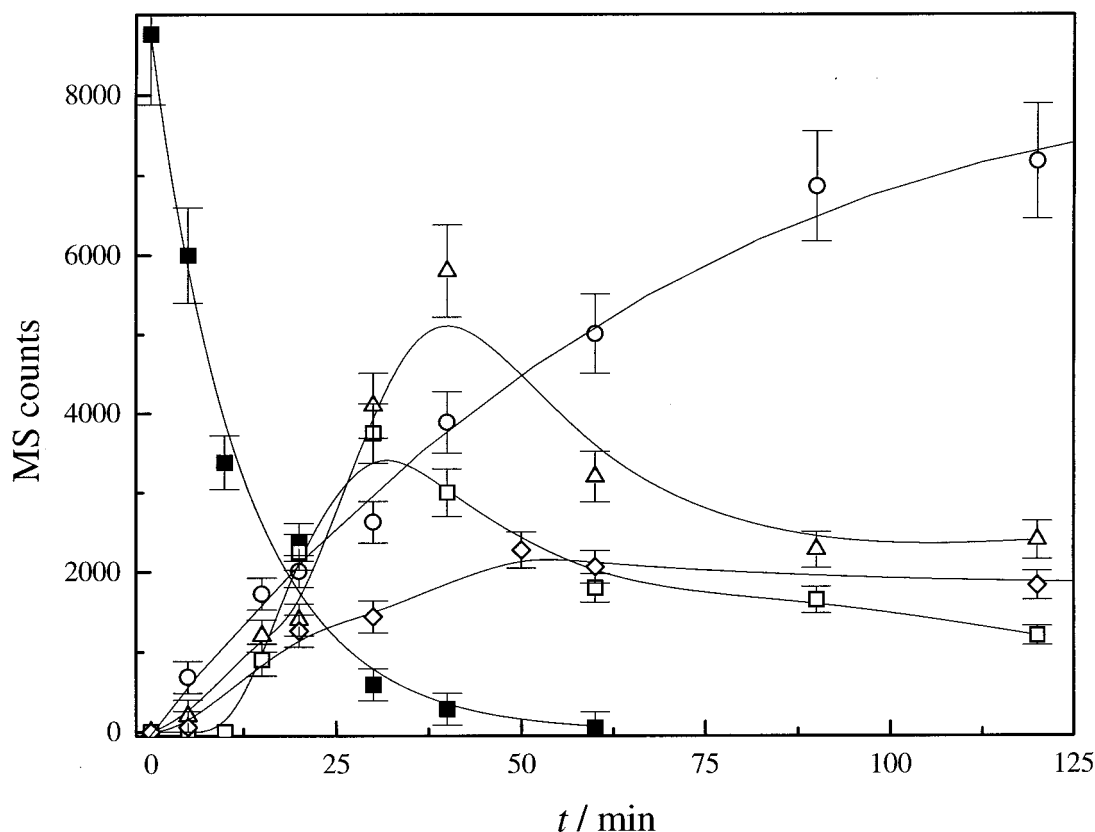
Figure 1. Depletion of *o*-methyl red (■) and variations in the observed concentrations of NO_3^- (○), benzoquinone (◇), nitrophenol (△) and dinitrobenzene (□) vs time during sonolyses at 500 kHz with an applied power of 50 W under Ar saturation.

TABLE 1: Spectroscopic Properties of the Studied Molecules

dye	azobenzene (AB)	methyl orange (MO)	*o*-methyl red (*o*-MR)	*p*-methyl red (*p*-MR)
λ nm	319	464	430	464
ϵ M-1 cm-1	22000	26900	20900	26300
pK_a		3.8	5.3	5.2

gas. In the presence of oxygen, other pathways different from •OH recombination also can lead to the formation of hydrogen peroxide, as shown below[7]

$$•H \, (g) + O_2 \, (g) + M \rightarrow HO_2• \, (g) + M \qquad (2)$$

$$2 \, HO_2• \, (g) \rightarrow H_2O_2 \, (g) + O_2 \, (g) \qquad (3)$$
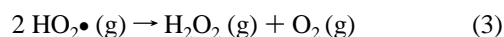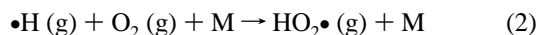
The target molecules studied in the present work are azobenzene (AB) and a group of monoazo dyes, which are structurally related (Table 1). Azo derivatives constitute a major part of all commercial dyes employed in a wide range of processes in the textile, paper, food, cosmetics, and pharmaceutical industries. They are characterized by the presence of the azo group (−N═N−) attached to two substituents, mainly benzene or naphthalene derivatives, containing electron withdrawing and/ or donating groups. The major sources of dyes in the environment are effluents from the textile industry. Due to their high solubility in water, they can be transported over very large distances once they are discharged into streams and rivers. Most of the dyes are found to be resistant to normal wastewater treatment processes, thus several methods have been developed to achieve their degradation, such as treatment with UV light in the presence of H_2O_2,[16,17] photocatalysis in aqueous TiO_2 suspensions,[18−21] conventional chemical methods,[22,23] gamma radiolysis techniques,[24] and ultrasonic irradiation.[25] The goal of these techniques is to eliminate the strong color of the effluents, which implies lowering of the concentration of the dye to under the ppm range. Azo compounds often become toxic to organisms after reduction and cleavage of the azo bond, for example due to the formation of aromatic amines via intestinal anaerobic bacteria.[26]

Experimental Methods

Aqueous solutions (10 μM) containing AB or the different dyes were prepared before each measurement and filtered

Sonochemical Degradation

J. Phys. Chem. A, Vol. 104, No. 2, 2000 **303**
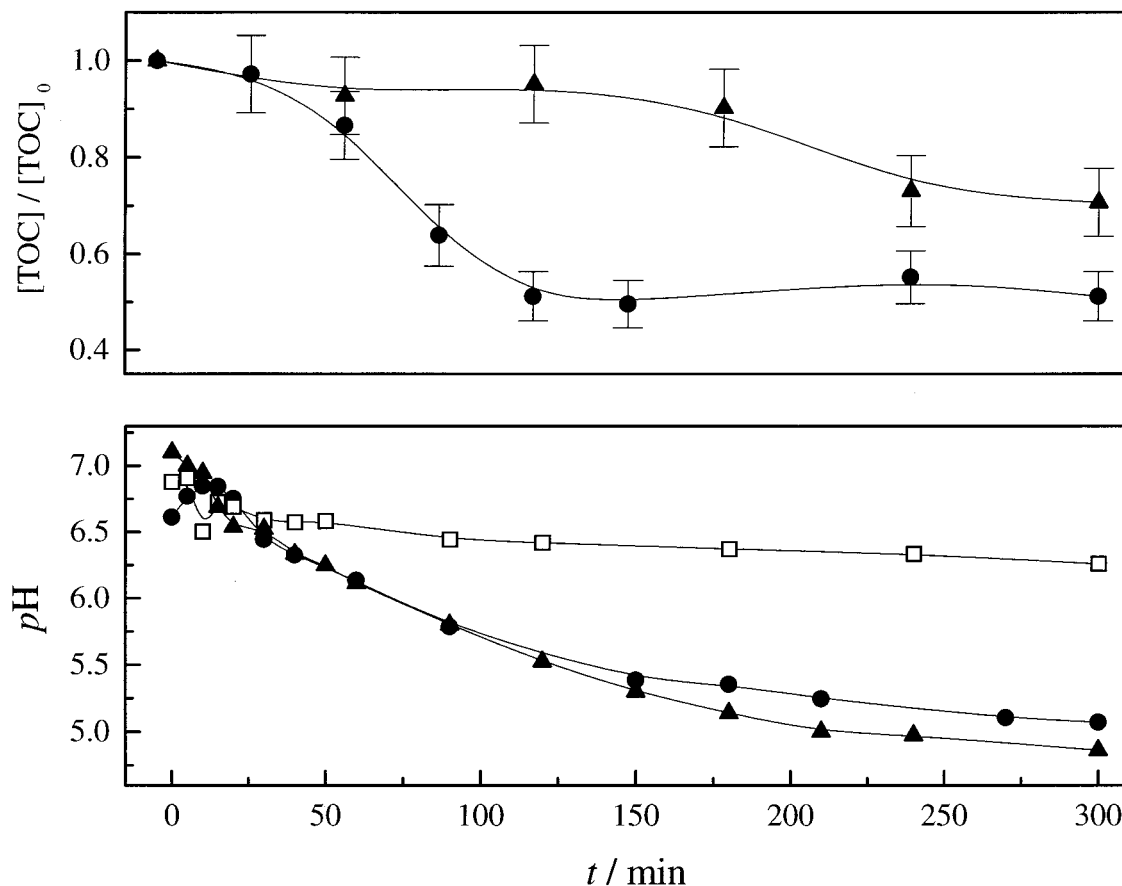
Figure 2. Relative TOC and pH profiles vs irradiation time for methyl orange (●) and azobenzene (▲) under Ar saturation. A blank for the pH measurements was also done in water (□).

through Millipore GS 0.22 μm disks. The concentrations were determined using the spectroscopic data presented in Table 1.[27,28] The high molar absorptivity values typical of these compounds allowed for experiments to be carried out at very low concentrations, to avoid the formation of dimers and also neglect the formation of complexes with the metal ions employed as catalysts. The pH of the solutions was measured using an Altex 71 pH meter.

The instrumentation employed in this study has already been described elsewhere.[3] The sonochemical reactor consisted of a 650 mL glass chamber surrounded by a self-contained water jacket and a piezoelectric transducer. Sonication at 500 kHz was performed with an ultrasonic transducer (Undatim Ultrasonics) operating at 50 W (2 W/cm^2). The ultrasonic power input to the reactor was determined using a standard calorimetric method.[29] The solution was stirred magnetically during each experiment and the temperature was kept constant at 15.0 ± 0.5 °C with a VWR Scientific thermostat. When the solutions were saturated with oxygen or argon, a stream of the gas was sparged into the reactor at a flow rate of 80 mL/min for 1 h before the reaction. For experiments conducted in the presence of Fe(II), the corresponding volume of a stock FeSO$_4$ solution (0.1 or 0.01 M) was injected into the solution before saturation with the respective gases. pH measurements were also performed under gas sparging.

Samples were collected for analysis at different times through a septum port by means of a syringe. The UV−vis absorption spectra were recorded using a Hewlett-Packard 8452 A diode array spectrophotometer. The analytical quantification of the products was carried out using a Hewlett-Packard 1100 HPLC system with UV detection and coupled to a mass spectrometer through an electrospray interface (ES-MS). The mass spectra

were recorded for both positive and negative ions in the range 50 to 1000 m/z units at 3 s/scan and a skimmer cone voltage of 3.5 kV. A 3 μm, 100 × 4 mm Hypersil BDS-C18 column (Hewlett-Packard) was used for MO, and a 5 μm, 100 × 2.1 mm Hypersil MOS-C8 column was used in the case of *o*-MR, *p*-MR, and AB. The eluent solution consisted of acetonitrile/ water mixtures in the proportion 15/85 for MO, 20/80 for *o*-MR, 10/90 for *p*-MR, and 50/50 for AB. The flow rate was 0.3 mL/ min in all cases. The wavelength used to follow the reduction in the dye concentrations was that corresponding to the maximum of the visible band as indicated in Table 1 for each dye. Total organic carbon (TOC) analyses were carried out with a Shimadzu 5000A TOC analyzer operating in the nonpurgable organic carbon (NPOC) mode. Calculations were performed with *Mathematica* 3.0.[30]

MO (Baker, >95%), *o*-MR (Sigma, >95%), *p*-MR (Sigma, >97%), AB (Aldrich, > 99%), and FeSO$_4$ (Fisher, 99%) were used without further purification. The solutions were prepared using water purified by a Millipore Milli-Q UV Plus system (R = 18.2 MΩ cm). The sparged gases (O$_2$ and Ar) were provided by Air Liquide.

Results and Discussion

Sonochemical Bleaching and Mineralization. The degradation of the azo compounds was studied following both the disappearance of the parent molecule (bleaching) and the degree of mineralization, as measured by the reduction of the total organic carbon present in the sample. Bleaching is a fast process, which is completed within the first 40 min of sonication, whereas mineralization is attained after a longer period of time. The nonvolatile nature of the azo dyes suggests that pyrolytic
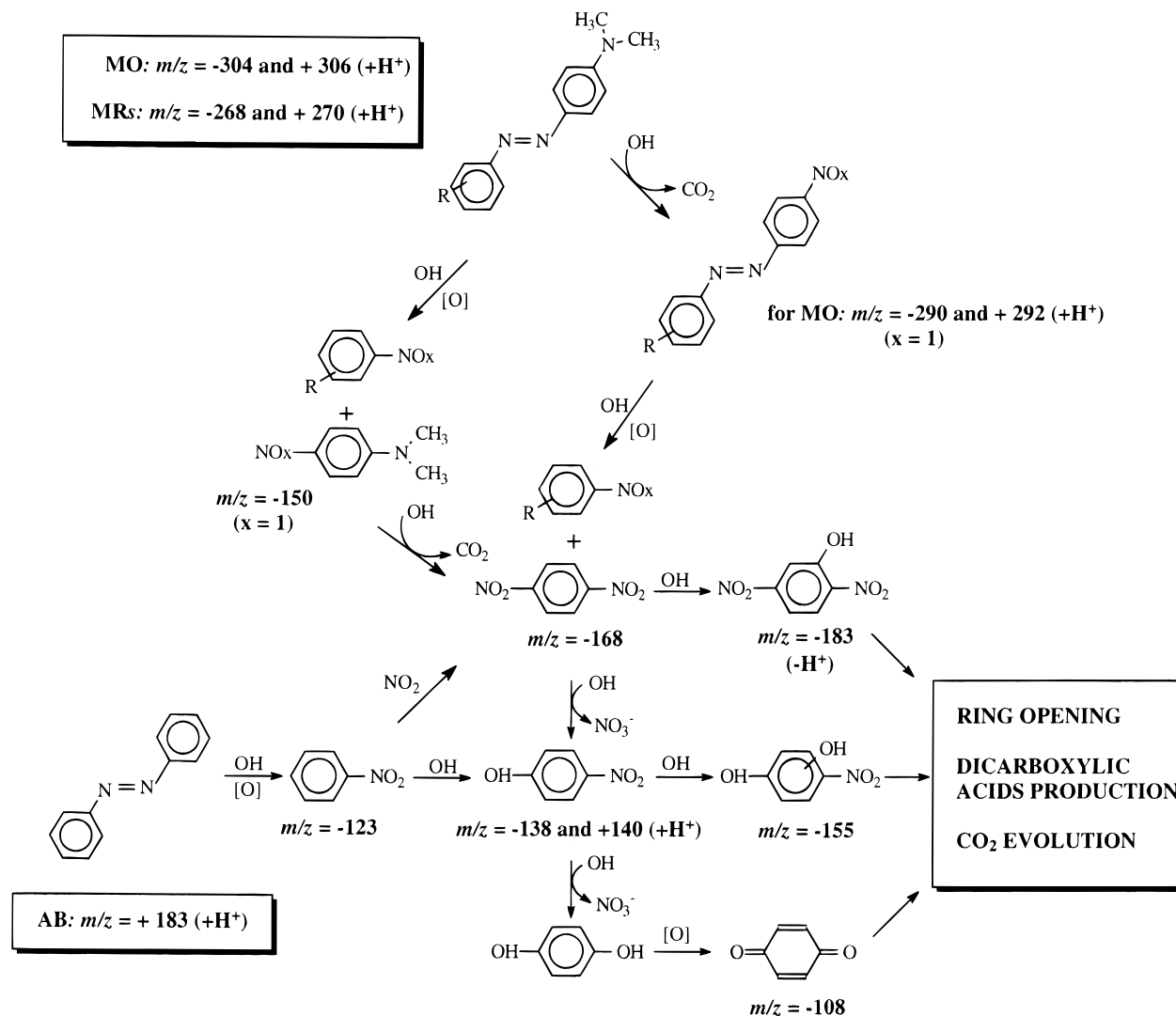
Figure 3. Main degradative pathways proposed for methyl orange, *o*- and *p*-methyl red, and azobenzene.

reactions within the collapsing bubbles can be negligible and that degradation occurs exclusively via the attack of hydroxyl radicals in the liquid phase. The absence of products generated in pyrolytic cleavage of the azo bond (with evolution of N_2) supports this contention, even for the slightly volatile AB. The fast bleaching, i.e., the decrease of the absorption band in the visible region, suggests that the addition of hydroxyl radicals to the azo double bond is one of the first steps in the degradation process, producing the loss of the chromophoric characteristic in the products and intermediates that are generated. Panajkar et al.[31] showed that •OH addition to the azo double bond is the main process (60%) in the radiolysis of this type of compound, while addition to aromatic rings accounts for the rest of the observed products.

The qualitative analyses by HPLC-ES-MS were performed under mild ionization conditions, thus the masses reported are those of molecules present in the sample, eventually protonated or deprotonated; no fragmentation was observed. The products identified are, then, the most reasonable guesses for a certain value of m/z. Irradiation under Ar, O_2, and air yielded similar product distributions for each dye. The fact that most of the intermediates and byproducts observed have a low molecular weight (i.e., contain only one aromatic ring) suggests that cleavage of the azo group is the first step in the overall degradation sequence. The anion nitrate ($m/z = -62$), which was detected from the beginning of the reaction in each case,

is one of the main reaction products. Successive addition of •OH to the nitrogen double bond and oxidation of the generated hydroxylamine (a reactive intermediate, which was not observed in the MS analysis) may be conducive to the final cleavage of the azo group, yielding two nitroso or nitro aromatic compounds. A portion of these products is able to partition within the gas phase inside the cavitation bubbles and undergo a fast pyrolytic decomposition yielding NO_2, which is further oxidized to yield NO_3^-.[32]

Some organic species have been identified through ES-MS as stable products present in the degradation of the azo dyes. They include acetic acid ($m/z = +60$), succinic acid ($m/z = +118$), benzoquinone ($m/z = +108$), and higher molecular weight dicarboxylic acids substituted with nitro groups ($m/z = -232$). A decrease of two pH units was observed after sonication in each case (see Figure 2), which is in agreement with the presence of HNO_3 and these organic acids as stable products.

Other intermediates were also identified. They include nitrobenzene ($m/z = -123$ and $+124$), dinitrobenzene ($m/z = -168$), nitrophenol ($m/z = +140$), nitrocatechol ($m/z = +155$), dinitrophenol ($m/z = -183$), and nitroso-*N,N*-dimethylaniline ($m/z = -150$). The low occurrence of dimethylanilines as intermediates indicates that the dimethylamino group, which is not present in AB, is also quite reactive under our experimental conditions. During the first 15 to 20 min of reaction, small amounts of an intermediate with an intact azo group were

Sonochemical Degradation

J. Phys. Chem. A, Vol. 104, No. 2, 2000 **305**

observed (for MO, $m/z = -290$ and $+292$). The production and depletion of some of the above intermediates and byproducts, together with the consumption of the parent molecule, are shown in Figure 1 for o-MR. The mass signal can be used in the present study only as a rough estimation of the amount of compound present at each time, since the sensitivity toward ionization in the electrospray process varies from one molecule to another. In the case of MO, the presence of a sulfonate group determined the existence of additional intermediates, such as hydroxybenzenesulfonate ($m/z = -173$) and nitrohydroxybenzenesulfonate ($m/z = -218$), while sulfate, which was present in the MS as HSO_4^-, $m/z = -97$, was found as the only byproduct containing sulfur. In the analysis of intermediates produced during the degradation of the MRs, aromatic carboxylic acids were observed. They included hydroxybenzoic acid ($m/z = -137$) and nitrohydroxybenzoic acid ($m/z = -182$).

The degree of mineralization was also studied as a function of the reaction time. The mineralization reaction can be represented as the complete oxidation of the parent molecule, as follows (in this example, for AB):

$$C_{12}H_{10}N_2 + 16.5 O_2 \xrightarrow{\bullet OH} 2NO_2 + 12CO_2 + 5H_2O \quad (4)$$

or

$$C_{12}H_{10}N_2 + 28 \bullet OH \xrightarrow{Ar} 2NO_2 + 12CO_2 + 19H_2 \quad (5)$$

In the case of MO and the MRs, after 90 to 120 min of continuous irradiation, the organic load remained constant in every case, reaching a limiting value of approximately 50% of the initial concentration (see Figure 2). This result is in agreement with the observed persistence of a variety of stable organic acids, quinones, and other species described above. Within the experimental error of the measurements (~10%, estimated from repeating calibrations in the concentration range of this work), no difference was observed in the mineralization process under air, O_2, or Ar. While mineralization of MO and the MRs presented similar characteristics, the process was much slower for AB. After 300 min, only 30% of the total organic matter present in the sample was destroyed. The reason for a slower mineralization is that the intermediates produced after the oxidative cleavage of the azo group of AB are essentially monosubstituted aromatic compounds (nitrobenzene). In the case of the other compounds, MO and the MRs, the oxidation of the disubstituted aromatic intermediates was easier and the amount of CO_2 produced was higher.[33]

The lowering of pH in parallel to the mineralization of MO and AB is also shown in Figure 2, together with a blank measurement, in an Ar-saturated solution. During the time of the initial bleaching reactions (i.e., the first 30 min), both the TOC concentrations and pH remained relatively constant. The production of stable organic acids accounts for the observed acidification of the sonicated solutions beyond the slight pH reduction observed in pure water irradiated in the same conditions. A similar behavior is observed under O_2. However, the pH of air-saturated solutions is lower due to the presence of dissolved CO_2.

Based on the above observations, a mechanistic scheme is presented in Figure 3 that illustrates some common degradative pathways for the studied dyes, including most of the observed byproducts.

Bleaching Kinetics. The depletion of the target molecules followed pseudo first-order kinetics with respect to the dye concentration. This suggests that a steady-state OH concentration
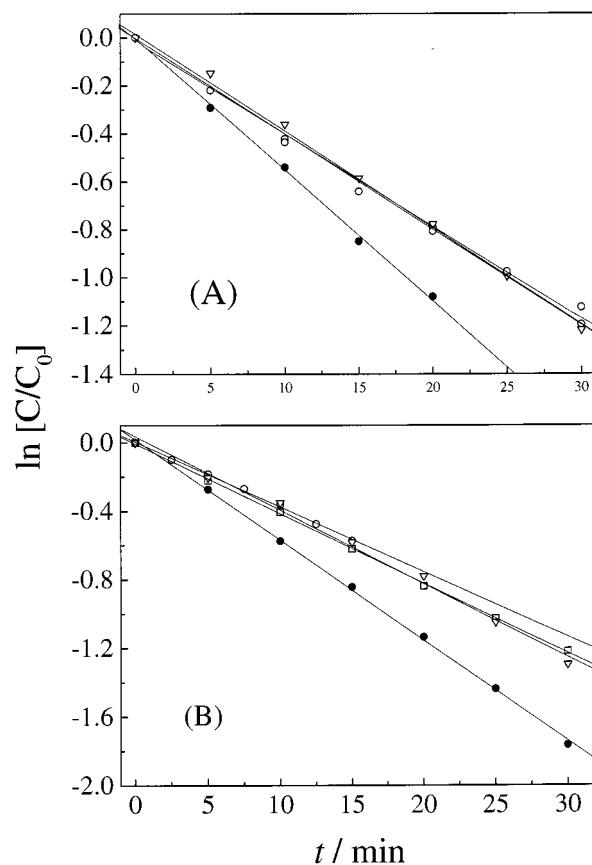
Figure 4. Sonochemical bleaching of azobenzene ($\square$), methyl orange ($\triangledown$), o-methyl red ($\bullet$), and p-methyl red ($\bigcirc$) under air (A) and Ar (B) saturation. Straight lines show the best fit in each case.

exists in the liquid phase under continuous irradiation. The resulting steady-state concentration depends in principle only on the nature of the saturation gas and the temperature.[1] The reduction in the concentration of the different substrate molecules is illustrated in Figure 4 for air- and Ar-saturated solutions. When the liquid was saturated with O_2, the observed trends were very similar to those shown in Figure 4(A). A similar reaction rate was observed for most of the dyes, indicating that the bleaching reaction

$$\text{dye (aq)} + \bullet OH \text{ (aq)} \rightarrow \text{products} \quad (6)$$
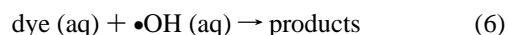
is relatively insensitive to the aromatic substitution in the *para* position. The faster process observed in the case of o-MR can be attributed to a positive substituent effect of the carboxylic group in the ortho position, near the azo group. Besides electronic effects, which undoubtedly can affect the reactivity of the azo group in this case, steric effects related to the proximity of the substituent in the opposite ring and the subsequent loss of planarity of the molecule may be responsible for the higher reactivity toward radicals when the N=N π overlap is reduced.

The observed pseudo first-order rate constants, k_i^{gas}

$$\frac{d[\text{dye}]}{dt} = k_i^{gas} [\text{dye}] \quad (7)$$

determined for the bleaching of the different compounds under air, O_2, and Ar are presented in Table 2. The experimental errors in the determination of the rate constant are also reported in Table 2. They were calculated from the value of the standard deviation of the linear regressions in Figure 4. Each reaction
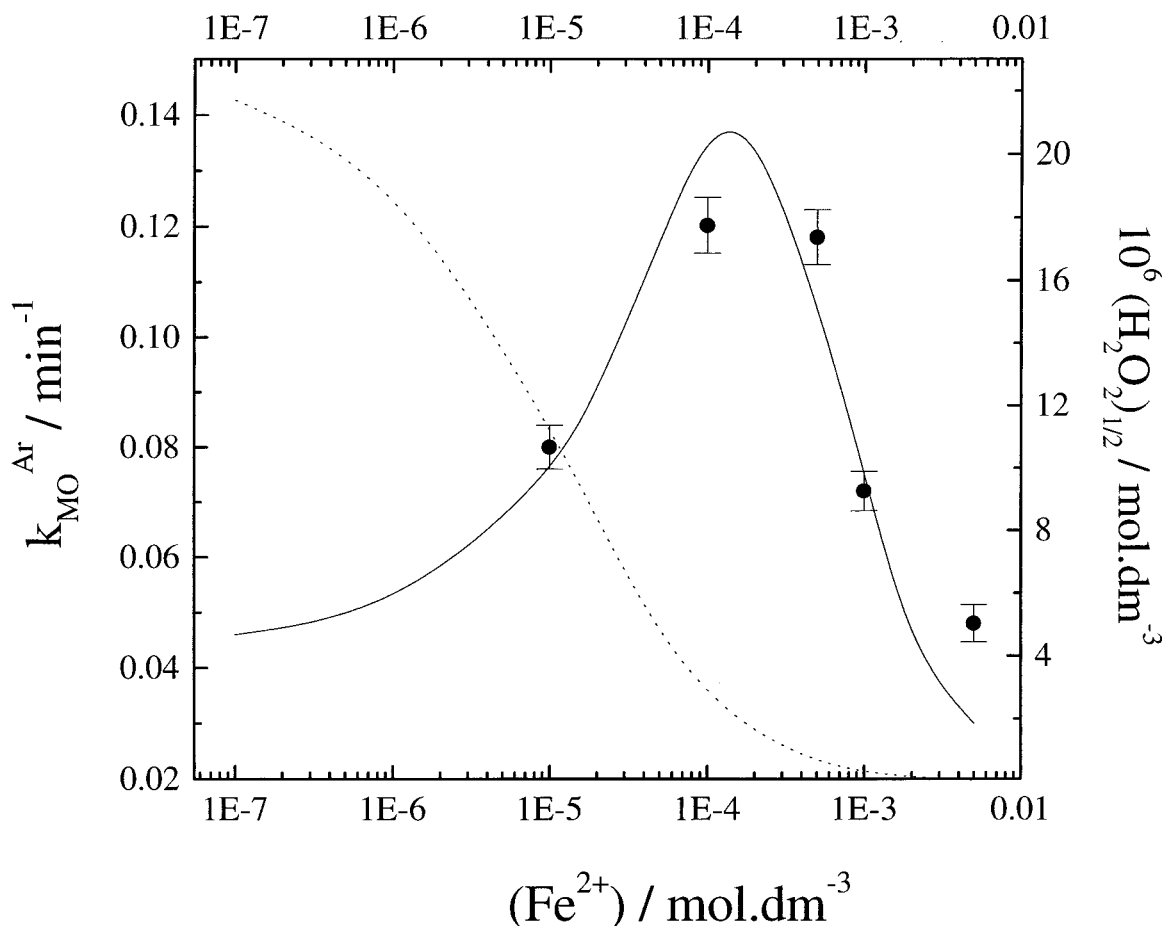
Figure 5. Effect of added Fe(II) on the pseudo first-order rate constant for the bleaching of methyl orange under Ar saturation (k_{MO}^{Ar}). The experimental values (●) were reproduced by adjusting the solution to eqs 10−13 (solid line). The amount of H_2O_2 produced when half of the MO is consumed, $(H_2O_2)_{1/2}$, is also shown (dashed line, scale on the right).

TABLE 2: Pseudo First-Order Rate Constants k_{dye}^{gas} for the Decolorization of 10 μM AB, MO, and MR (*p*- and *o*-) under Different Gas Saturation

| dye	k_{dye}^{air}/min^{-1}	$k_{dye}^{O_2}$ /min^{-1}	k_{dye}^{Ar}/min^{-1}
AB	0.042 ± 0.002	0.043 ± 0.002	0.049 ± 0.002
MO	0.040 ± 0.002	0.042 ± 0.002	0.046 ± 0.002
p-MR	0.035 ± 0.002	0.033 ± 0.002	0.043 ± 0.002
o-MR	0.054 ± 0.002	0.053 ± 0.002	0.059 ± 0.003

was repeated 2 or 3 times, the value of k_i^{gas} being within the reported error margin in every case. In each case, the use of Ar as a background gas enhances the value of k_i^{Ar} by 10% compared to k_i^{air} and $k_i^{O_2}$. This observation is consistent with a previous report by Hua and Hoffmann[9] where, at a similar frequency (513 kHz), an 8% increase was observed in the production of •OH when the solutions were saturated with Ar instead of O_2. The enhancement in the reaction rate when the background gas is changed correlates linearly with an increment in the steady-state concentration of •OH.

Catalysis with Fe(II). The enhancement of the bleaching reaction rate in the presence of Fe(II) ions was investigated as a function of the concentration of FeSO$_4$ in the range 10 μM to 5 mM. The lower Fe(II) concentrations had a minor effect, while the upper concentration limit was established by the precipitation threshold of iron oxides during the reaction. All of the kinetic measurements for this system were carried out with 10 μM MO solutions, in the absence of iron oxides precipitation, and under Ar saturation. Figure 5 illustrates the changes observed in the apparent first-order rate constants k_{MO}^{Ar} when the experiments were carried out in the presence of different Fe(II) concentra-

tions. A maximum 3-fold increase in the measured rate constant was observed when the Fe(II) concentration was between 0.1 mM and 0.5 mM. This increment was due to the higher •OH radical concentration produced through Fenton's reaction (eq 1). Further increases in [Fe(II)] showed no further catalytic activity, due to the direct reduction of •OH radicals by the metal ions

$$Fe^{2+} (aq) + \bullet OH (aq) \rightarrow Fe^{3+} (aq) + OH^- (aq) \quad (8)$$
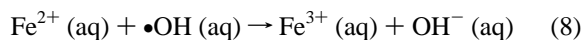
A kinetic model based on a simple reaction scheme in the bulk liquid phase, considering only eqs 1, 6, 8, and the •OH radical recombination in solution,

$$2 \bullet OH (aq) \rightarrow H_2O_2 (aq) \quad (9)$$
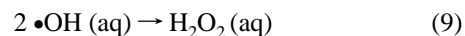
is able to reproduce our experimental observations. This model represents an oversimplification of the real case, since the •OH attack on byproducts and intermediates is not considered in the calculations and the direct reaction of the dye with H_2O_2 is also ignored.[34] Scavenging of •OH radicals by hydrogen peroxide was initially included, but that reaction is not significant in the present conditions. The primary sonochemical process, i.e., the production of active species by the cavitating bubbles and their release in solution, is included in the model as a zero-order kinetic process. We only consider the bubble output of •OH and H_2O_2, because H• recombination in the gas phase is highly effective in the absence of O_2, when reactions 2−3 cannot take place.[15] For the same reason, the only source of H_2O_2 under Ar is the recombination of •OH radicals both in the gas phase and

Sonochemical Degradation

J. Phys. Chem. A, Vol. 104, No. 2, 2000 **307**

TABLE 3: Values of the Rate Constants Employed in Equations 10−13

constant	ref
$k_{OH} = 5.5 \ 10^{-9} \ Ms^{-1}$	
$k_{H_2O_2} = 2.4 \ 10^{-8} \ Ms^{-1}$	
$k_1 = 76 \ M^{-1} \ s^{-1}$	36
$k_6 = 2 \ 10^{10} \ M^{-1} \ s^{-1}$	39
$k_8 = 3 \ 10^8 \ M^{-1} \ s^{-1}$	35
$2k_9 = 1.1 \ 10^{10} \ M^{-1} \ s^{-1}$	35

during the dissolution process after the cavity implosion. The values of the zero-order constants for the •OH (aq) and H_2O_2 (aq) sonochemical production, k_{OH} and $k_{H_2O_2}$, are the adjustable parameters of the model, related with the density and rate of bubble implosions, and with their capability to release •OH and H_2O_2 in solution.

The differential eqs 10−13 describe the concentration changes of the species involved in the liquid phase. The values of the kinetic constants employed are presented in Table 3. Although these literature values are reported at 25 °C and not at our work temperature (15 °C), we assume that differences may be negligible since the temperature dependence of diffusion control rates in reactions involving radicals (eqs 6, 8, and 9) is minor. In the case of the Fenton's reaction (eq 1), reported experimental results also support this assumption.[38]

$$\frac{d[\bullet OH]}{dt} = k_{OH} - k_6[MO][\bullet OH] - k_9[\bullet OH]^2 +$$
$$k_1[Fe^{2+}][H_2O_2] - k_8[Fe^{2+}][\bullet OH] \quad (10)$$

$$\frac{d[MO]}{dt} = -k_6[MO][\bullet OH] \quad (11)$$

$$\frac{d[H_2O_2]}{dt} = k_{H_2O_2} + k_9[\bullet OH]^2 - k_1[Fe^{2+}][H_2O_2] \quad (12)$$

$$\frac{d[Fe^{2+}]}{dt} = -k_1[Fe^{2+}][H_2O_2] - k_8[Fe^{2+}][\bullet OH] \quad (13)$$

Figure 5 illustrates the calculated curve fitted to the experimental data, when the values for k_{OH} and $k_{H_2O_2}$, which are reported in Table 3, were used. The sonochemical output of H_2O_2 predicted is four times higher than the value for •OH, again in good agreement with the experiments of Hua and Hoffmann[9] (a factor of 5 both in Ar and O_2). These results reveal the magnitude of the improvement in the sonochemical efficiency that can be theoretically achieved if the •OH recombination can be partially diverted by Fenton-like reactions. The rate of H_2O_2 production is also represented in Figure 5 by $(H_2O_2)_{1/2}$, the concentration of H_2O_2 reached when the dye concentration was reduced to a half of the initial value. Over the range of Fe(II) concentrations investigated, a 2 order of magnitude decrease in the production of H_2O_2 is predicted by the model.

The effect of Fe(II) on the yields of mineralization was also analyzed. In the presence of 0.1 mM Fe(II), the final limiting value for total organic carbon depletion was the same as that observed in the absence of the metal ions (50%), but this final state was reached much faster (only 20 min, versus 120 in the absence of iron, see Figure 2). Thus, the extent of mineralization was not increased. However, the velocity at which the limit level is reached is increased in the presence of Fe(II). When the concentration of Fe(II) was lower or higher than that optimum value, the mineralization curves were similar to those recorded in the absence of the metal ions. A complete mineralization of the sample can only be attained by combining ultrasonic

irradiation with the addition of strong oxidants such as O_3, which are able to attack some of the remaining stable organic compounds (i.e., benzoquinone and organic acids).[37] Preliminary results from ongoing work in our lab support this assumption.

References and Notes

(1) Mason, T. *Sonochemistry. Theory, Applications and Uses of Ultrasound in Chemistry*; Wiley: New York, 1988.

(2) Hoffmann, M. R.; Hua, I.; Hochemer, R.; Willberg, D.; Lang P.; Kratel, A. In *Chemistry Under Extreme Non-Classical Conditions*; van Eldik, R., Hubbard, C. D., Eds.; Wiley & Sons: New York, 1997; chapter 10.

(3) Hung, H. M.; Hoffmann, M. R. *J. Phys. Chem A*, **1999**, *103*, 2734.

(4) Destaillats, H.; Hung, H. M.; Hoffmann, M. R. *Environ. Sci. Technol*. in press.

(5) Weaver, L. K.; Ling, F. H.; Hoffmann, M. R. *Environ. Sci. Technol*, **1998**, *32*, 2727.

(6) Leighton, T. G. *The Acoustic Bubble*; Academic Press: London, 1992.

(7) Colussi, A. J.; Weavers, L. K.; Hoffmann, M. R. *J. Phys. Chem A*, **1998**, *102*, 6927.

(8) Didenko, Y. T.; McNamara, W. B., III; Suslick, K. S. *J. Am. Chem. Soc*. **1999**, *121*, 5817.

(9) Hua I.; Hoffmann, M. R. *Environ. Sci. Technol*. **1997**, *31*, 2237.

(10) Kawabata K.; Umemura, S. *J. Phys. Chem*. **1996**, *100*, 18784.

(11) Hua, I.; Hochemer R. H.; Hoffmann, M. R. *Environ. Sci. Technol*. **1995**, *29*, 2790.

(12) Olson, T. M.; Barbier, P. F. *Water Res*. **1994**, *28*, 1383.

(13) Isaacs, N. S. *Physical Organic Chemistry*; Longman: London, 1987; p 719.

(14) Barbeni, M.; Minero, C.; Pelizzetti, E.; Borgarello E.; Serpone, N. *Chemosphere* **1987**, *16*, 2225.

(15) Hart, E. J.; Henglein, A. *J. Phys. Chem*. **1985**, *89*, 4342.

(16) Ince, N. H. *Water Res*. **1999**, *33*, 1080.

(17) Shu, H. Y.; Huang, C. R.; Chang. M. C. *Chemosphere,* **1994**, *29*, 2597.

(18) Nasr, C.; Vinodgopal, K.; Fisher, L.; Hotchandani, S.; Chattopadhyay, A. K.; Kamat. P. V. *J. Phys. Chem*. **1996**, *100*, 8436.

(19) Vinodgopal, K.; Wynkoop, D. E.; Kamat, P. V. *Environ. Sci. Technol*. **1996**, *30*, 1660.

(20) Lagrasta, C.; Bellobono, I. R.; Bonardi, M. *J. Photochem. Photobiol A*; Chemistry, **1997**, *110*, 201.

(21) Chen, L. C.; Chou, T. C. *J. Mol. Catal*. **1993**, *85*, 201−214.

(22) Tang, W. Z.; Chen, R. Z. *Chemosphere* **1996**, *32*, 947.

(23) Spadaro, J. T.; Isabella, L.; Renganathan, V. *Environ. Sci. Technol*. **1994**, *28*, 1389.

(24) Ravishankar, D.; Raju, B. *J. Radioanal. Nucl. Chem. Articles*, **1994**, *178*, 351.

(25) Vinodgopal, K.; Peller, J.; Makogon, O.; Kamat, P. V. *Water Res*. **1998**, *32*, 3646.

(26) Glezer, V. In *The Chemistry of the Hydrazo, Azo and Azoxy Groups*; Patai, S., Ed.; Wiley & Sons: New York, 1997; p 729.

(27) Graselli, J. G., Ed. *Atlas of Spectral Data and Physical Constants for Organic Compounds*, CRC Press: Ohio, 1973.

(28) Phillips J. P.; Freedman, L. D.; Cymerman, J., Eds.; *Organic Electronic Spectral Data*; Wiley-Interscience: New York, 1973 Vol. VI.

(29) Mason, T. J. *Practical Sonochemistry: User's Guide to Applications in Chemistry and Chemical Engineering*; Ellis Horwood: England, 1991.

(30) Wolfram, S. *Mathematica*; Wolfram Media and Cambridge University Press, 1996

(31) Panajkar, M. S.; Mohan, H. *Indian J. Chem*. **1993**, *32 A*, 25.

(32) Kotronarou, A.; Mills, G.; Hoffmann, M. R. *J. Phys. Chem*. **1991**, *95*, 3630−3638.

(33) Berlan, J.; Trabelsi, F.; Delmas, H.; Wilhelm A. M.; Petrignani, J. F. *Ultrasonics Sonochemistry*, **1994**, *1*, S97.

(34) Shu, H. Y.; Huang, C. R.; Chang, M. C. *Chemosphere* **1994**, *29*, 2597.

(35) Buxton, G. V.; Greenstock, C. L.; Helman, W. P.; Ross, A. B. *J. Phys. Chem. Ref. Data*, **1988**, *17*, 513.

(36) Walling, C. *Acc. Chem. Res*. **1975**, *8*, 125.

(37) Kang, J. W.; Hoffmann, M. R. *Environ. Sci. Technol*. **1998**, *32*, 3194.

(38) Solozhenko, E. G.; Soboleva, N. M.; Goncharuk, V. V. *Water Res*. **1995**, *29*, 2206.

(39) Padmaja, S.; Madison, S. A. *J. Phys. Org. Chem*. **1999**, *12*, 221.